

# RSC Advances



This is an *Accepted Manuscript*, which has been through the Royal Society of Chemistry peer review process and has been accepted for publication.

*Accepted Manuscripts* are published online shortly after acceptance, before technical editing, formatting and proof reading. Using this free service, authors can make their results available to the community, in citable form, before we publish the edited article. This *Accepted Manuscript* will be replaced by the edited, formatted and paginated article as soon as this is available.

You can find more information about *Accepted Manuscripts* in the [Information for Authors](#).

Please note that technical editing may introduce minor changes to the text and/or graphics, which may alter content. The journal's standard [Terms & Conditions](#) and the [Ethical guidelines](#) still apply. In no event shall the Royal Society of Chemistry be held responsible for any errors or omissions in this *Accepted Manuscript* or any consequences arising from the use of any information it contains.

## ARTICLE

# Morphological Control of Mesoporous CN Based Hybrid Materials and their Excellent CO<sub>2</sub> Adsorption Capacity

Cite this: DOI: 10.1039/x0xx00000x

Received 00th January 2012,  
Accepted 00th January 2012

DOI: 10.1039/x0xx00000x

Kripal S. Lakhi,<sup>a</sup> Arun V. Baskar,<sup>a</sup> Javaid S.M. Zaidi,<sup>a</sup> Salem S. Al-Deyab,<sup>b</sup>  
Mohamed El-Newehy,<sup>b</sup> Jin-Ho Choy,<sup>c</sup> and Ajayan Vinu<sup>a\*</sup>

Highly ordered mesoporous carbon nitrides (MCN-1-Ts) with uniform rod shaped morphology have been synthesized by hard templating technique using SBA-15 silicas prepared under hydrothermal “static” condition at different temperatures as templates following a simple polymerization reaction between carbon tetrachloride (CTC) and ethylenediamine (EDA) inside the large pores of SBA-15. The static hydrothermal condition offers uniform rod shaped morphology for the template materials which has been completely replicated into the MCN nanostructures. The obtained materials were characterized with low angle XRD, N<sub>2</sub> adsorption, high resolution transmission electron microscopy, high resolution scanning electron microscopy (FE SEM), Fourier transform infra-red (FT-IR), and X-ray photoelectron spectroscopy (XPS). The characterization results confirm the successful replication of the ordered structure, morphology and mesoporosity of the template material into carbon nitride. The FT-IR and XPS techniques confirm the presence of free –NH and –NH<sub>2</sub> groups on the surface of MCN, which are critical for capturing CO<sub>2</sub>. Finally, these materials with high surface area and uniform morphology are used as adsorbents for high pressure CO<sub>2</sub> adsorption at different temperatures of 0, 10 and 25 °C. It is found that the morphology of the materials which has a direct relation with the textural parameters plays a significant role in enhancing the amount of CO<sub>2</sub> adsorption. The MCN with the uniform morphology and the highest surface area registers the highest CO<sub>2</sub> adsorption capacity (16.5 mmol/g) at 0 °C and 30 bar pressure, which is found to be higher than that of previously reported 3D- cage type MCN, activated carbon, multiwalled carbon nanotube and mesoporous silicas.

## 1. Introduction

The rapid increase in CO<sub>2</sub> levels due to wide spread industrialization and human activities in both developed and developing countries is posing a potential threat to severe climatic conditions in the form of global warming, floods, melting of glaciers, drought and other natural events. CO<sub>2</sub> is produced as a by-product in a number of processes but two prominent ones are burning of fossil fuels for power generation and the transportation industry. It is reported that CO<sub>2</sub> alone contributes 60% of the total global warming caused by all the greenhouse gases put together [1]. At the same time, CO<sub>2</sub> has been viewed by the scientific community as a potential source for production of useful chemicals and efficient transport fuels such as methanol, dimethyl ether and their useful derivatives [2]. Therefore, researchers put a lot of efforts to find solutions not only to reduce the CO<sub>2</sub> emission to the atmosphere but also its conversion to value added products.

Carbon capture and sequestration is being developed as a promising technology to reduce large scale CO<sub>2</sub> emission particularly from coal fired power plants and all efforts are being made to make processes green and environmentally friendly. Although many physical and chemical absorption based technologies are available, the most common CO<sub>2</sub> capture technology in use today is the absorption in liquid amine and ammonia solution. However, the liquid ammonia absorption process has a number of disadvantages such as high regeneration cost, corrosion of equipment, hazardous nature etc. A number of solid adsorbents including a wide range of porous materials such as metal organic frameworks (MOFs), activated carbon, porous carbon, amine-functionalized porous silica, functionalized porous carbons, zeolites, porous polymers have been tried as possible adsorbents for CO<sub>2</sub> [2-4]. Among these adsorbents, porous carbon materials are considered as the best candidates due to their low cost, ease of preparation and regeneration, high surface area, excellent thermal and chemical stability. However, they suffer from poor CO<sub>2</sub> adsorption capacities due to weaker adsorbate-adsorbent interaction

resulting primarily from the hydrophobic and neutral surface charge [4]. Therefore, much efforts have been given to the functionalization of porous carbon adsorbents with N atoms or basic molecules which enhances the adsorption of CO<sub>2</sub> due to the acid-base interaction [5-7].

Zhao et al. used the post-synthetic approach to incorporate N atoms on the 3D nanoporous carbon framework by treating with melamine precursor, which showed the maximum CO<sub>2</sub> adsorption capacity of 8.5 mmol/g at 15 °C and 10 bar pressure [8] whereas Zhu et al. reported the N-doped porous carbons from expensive ionic liquids, which registered the CO<sub>2</sub> adsorption capacity of 4.39 mmol/g at 0 °C and 1 bar [9]. Ahn et al. introduced polyethylenimine (PEI) inside the porous channels of mesoporous silicas such as SBA-15, SBA-16, KIT-6, MCM-48 and MCM-41 in order to enhance the amount of CO<sub>2</sub> adsorption [10]. However, these approaches require either additional steps or expensive nitrogen precursors for introducing the basic sites on the surface of the porous adsorbents which increases the cost of the materials and thereby presents a major hurdle for the practical applications.

Carbon nitride (CN) is a unique material with excellent electronic and electrical properties. The surface properties of CN are quite different from those of pure carbon materials as the incorporation of nitrogen atoms in the carbon nanostructure can enhance the mechanical, conducting, and semiconducting properties and further offer basic sites on the surface. Recently, Vinu et al. have introduced mesoporosity in the CN through a combined nanohard templating and a simple polymerization technique by mixing ethylenediamine and carbon tetrachloride inside the nanochannels of the mesoporous SBA-15 template [11-12]. These materials have excellent properties such as strong basicity, inherent semiconducting nature, large surface area, high pore volume, controllable pore size and excellent thermal and mechanical stability, which may be utilized for various applications including adsorption, separation, and catalysis [11-12]. Especially, mesoporous carbon nitride based hybrids (MCN) are particularly attractive for capturing acidic CO<sub>2</sub> molecules because the free NH<sub>2</sub> groups on its surface can selectively adsorb the CO<sub>2</sub> molecules through acid-base interaction [13].

Morphology and textural parameters of the mesoporous materials are extremely important for many applications including adsorption and catalysis as they dictate surface area and pore volume and offer easy access to the active sites and support the inter-particle diffusion. In the nano-hard templating approach, in general, the structure of the template is inversely replicated and the particle morphology is retained into the desired materials. Therefore, it is important to find a suitable method to control the morphology of the template materials. For tuning the morphology of MCN, it is necessary to find a method to control the morphology of the template first as it directs the morphology of the replicated material. It has been widely reported that the morphology of the mesoporous silica materials can be controlled by altering the nature of the surfactants, cosolvents or the additives such as KCl or NH<sub>4</sub>F or (NH<sub>4</sub>)<sub>2</sub>SiF<sub>6</sub> [14-16]. By varying the synthesis conditions, various morphologies of mesoporous silica including rod, sphere, fibre, platelet, groid, discoid, doughnut, sausage etc have been prepared. For example, Kosuge et al. reported fibre and rod like SBA-15 mesoporous silica using the inexpensive sodium silicate which served both as a silica source as well as the salt [17]. Although there are several methods available in the literature to control the morphology of the mesoporous silica materials, the use of "static" synthesis condition, reported by Sayari [18] and his co-workers to prepare the mesoporous silica with a highly uniform and well-defined rod shaped morphology has been found to be the best as it is considered an easy, salt-free and inexpensive approach.

In the hard templating approach, the walls and the pores of the inorganic porous templates are converted into pores and walls of the final product, respectively. However, the final product retains the

morphology of the inorganic template. Thus, it is important to control the morphology of the template in order to prepare the materials with different morphology using hard templating approach. With this approach, several nanoporous carbons with different pore diameters and particle morphology have been prepared [19]. Previously, Vinu et al. have also used mesoporous silica with tunable pore diameters and/or particle morphology to fabricate a series of mesoporous carbon materials which showed excellent adsorption capacity for biomolecules including proteins, vitamins and aminoacids [19-26]. However, there is no report available in the literature on controlling the particle morphology of the mesoporous carbon nitride materials.

In this work, we report on the synthesis of highly ordered MCNs with a high nitrogen content and controlled morphology using SBA-15 silica materials with uniform rod shaped morphology prepared under "static condition" as templates and ethylene diamine and carbon tetrachloride as the carbon and nitrogen sources, respectively. The materials exhibit a high structural order with well-defined cylindrical or rod shaped particle morphology and excellent textural parameters. We also show that the MCNs prepared with controlled morphology can be used as the adsorbents for CO<sub>2</sub> molecules. The CO<sub>2</sub> adsorption capacity was found to be ca 726 mg/g (16.5 mmol/g) of the adsorbent at 273K which is much higher than that reported for other MCN [13], activated carbons, multi-walled carbon nanotubes, N-doped porous carbons [8,9] and pure and functionalized mesoporous silica materials [10]. The reason for the higher CO<sub>2</sub> adsorption capacity of these MCN with controlled morphology, and the mechanism and the heat of adsorption have also been discussed in detail.

## 2. Experimental

### 2.1 Synthesis

The mesoporous SBA-15 silica template material was synthesized under static condition using a soft templating approach under strongly acidic condition. In a typical synthesis, 4 g of non-ionic surfactant Pluronic P-123 which is a triblock copolymer (EO<sub>20</sub> PO<sub>70</sub> EO<sub>20</sub>), Avg. mwt ~5800, Sigma-Aldrich) was added to 30 g of water in a polypropylene (PP) bottle with a cap. After being stirred continuously for 4 h, 120g of 2M HCl was added to the solution. The temperature was simultaneously raised to 40 °C and the mixture was stirred for 2 h. Subsequently, 9 g of TEOS (tetraethyl orthosilicate, 98% Sigma-Aldrich) was added and the mixture was stirred for only 20 min after which stirring was stopped completely and the sample was left unagitated for the next 24 h with the temperature in the water bath maintained at 40 °C. The solution mixture was then transferred to a Teflon lined autoclave and kept in an oven at 100 °C for 48 h. The resulting product was filtered in hot, washed three times with a large amount of water, dried at 100 °C for 6 h and calcined at 540 °C for 12 h to remove the polymeric surfactant. Another set of mesoporous silica templates was prepared by using the above procedure except that autoclaving was done at 130 °C and 150 °C. The obtained samples were labeled as SBA-15-Ts where T is the hydrothermal synthesis temperature and S denotes static conditions.

MCN was prepared using a hard templating approach involving a polymerization reaction between the carbon source, CCl<sub>4</sub>, and the nitrogen source, ethylenediamine, inside the mesopores of the SBA-15-Ts materials. In a typical synthesis, 0.5 g of SBA-15-Ts was mixed with 3 g of CCl<sub>4</sub> and 1.35 g of ethylenediamine in a round bottom flask fitted with water cooled condenser. The mixture was refluxed at 90 °C for 6 h under constant stirring. The temperature was increased in steps of 10 °C from 60 to 90 °C. After 6 h of stirring at 90 °C, the unreacted CCl<sub>4</sub> and ethylenediamine in the composite polymer was removed using the rotavapor at 55 °C. The sample was then dried at 100 °C for 6 h and then crushed into fine powder using a mortar and pestle. The crushed powder was then carbonized in a tubular furnace

at 500 °C for 6 h under nitrogen flow. The carbonized sample was then treated with 5% HF and the sample was washed three times with excess ethanol and then kept for drying at 100 °C for 6 h. The samples were labelled as MCN-1-Ts where T denotes the synthesis temperature of the template.

## 2.2 Characterization

The powder X-ray diffraction measurements were carried out on a *Bruker Advance D8-III* diffractometer using Cu K $\alpha$  radiation from a sealed tube source operating at 40 kV and 40 mA, a fixed divergence slit of 0.1° and a *Lynxeye* multi-pixel detector. The data were recorded in a 2 $\theta$  range from 0.5 to 8° with a scan rate of 0.01°/sec. Nitrogen adsorption and desorption isotherms were measured at -196 °C on a Micromeritics ASAP 2420 surface area and porosity analyser. All the samples were separately degassed at 250 °C for 8 h under vacuum in the degas port of the adsorption analyser. The specific surface area was calculated using the BET model. Pore size distribution was obtained from both the adsorption and desorption branch of the nitrogen isotherms using the BJH model.

X-ray photoelectron spectroscopy was carried out using a Kratos Axis ULTRA X-ray photoelectron spectrometer incorporating a 165mm hemispherical electron energy analyser using monochromatic Al K $\alpha$  X-rays (1486.6eV) at 225W (15kV, 15ma). Survey and multi-region spectra were recorded at C1s and N1s photoelectron peaks. Each spectra region of photoelectron of interest was scanned several times to obtain a good signal to noise ratios. Survey (wide) scans were taken at analyser pass energy of 160eV and multiplex (narrow) high resolution scans at 20eV. Survey scans were carried out over 1200-0eV binding energy range with 1.0eV steps and a dwell time of 100ms. Narrow high-resolution scans were run with 0.05eV steps and 250 ms dwell time. Atomic concentrations were calculated using the CasaXPS version 2.3.14 software and a Shirley baseline with Kratos library Relative Sensitivity Factors (RSFs). Peak fitting of the high-resolution data was also carried out using the CasaXPS software. FT-IR spectra were recorded on a Nicolet 5700 FTIR spectrometer fitted with a diamond attenuated total reflection (ATR) accessory by averaging 200 scans with a resolution of 2 cm<sup>-1</sup> measured in absorbance mode.

High pressure CO<sub>2</sub> adsorption was carried out on a Quantachrome Isorb HP1 equipped with temperature controlled circulator and a booster compressor. The CO<sub>2</sub> adsorption was carried out in the pressure range of 0 to 30 bar and different analysis temperatures from 0 to 25 °C were used. Prior to CO<sub>2</sub> adsorption, samples were degassed under vacuum at 250 °C for 8 h. The isosteric heat of adsorption was calculated using Clausius-Clapeyron equation. The structural morphology of MCN-1-Ts samples was observed on a JEOL FE SEM 7001 whereas the HR-TEM images were obtained using a Tecnai F20 FEG TEM equipped with EDAX EDS and GIF (Gatan Image Filter). The preparation of the samples for HR-TEM imaging involved sonication of 10-15 mg of the sample in ethanol for 5 to 8 min and deposition on a holey carbon film supported copper grid.

## 3. Results and Discussion

Mesoporous silica materials with rod shaped morphology were prepared using polymeric surfactants under static conditions. The structure of the prepared template materials was first confirmed by powder X-ray diffraction analysis. **Figure 1a** shows the low angle powder XRD patterns for the SBA-15-Ts template materials. All the XRD patterns exhibit several well-ordered peaks which can be indexed as (100), (110) and (200) reflection planes on a two-dimensional hexagonal lattice (*p6mm*) and are characteristic low angle peaks for the silica SBA-15 materials and consistent with the reports available in the literature [11,12,27]. These results reveal that the static condition did not affect the structural order of SBA-15 materials

prepared at different temperatures. Further, it is observed that diffraction peaks shifted to lower angles with increase of hydrothermal temperature, which indicates the increase in d spacing and the unit cell size. The values of cell constant and d<sub>100</sub> spacing show an increasing trend as the synthesis temperature is increased from 100 through 150 °C (**Table 1**). Similar results were also reported previously for the SBA-15 samples prepared under dynamic conditions [11-12].

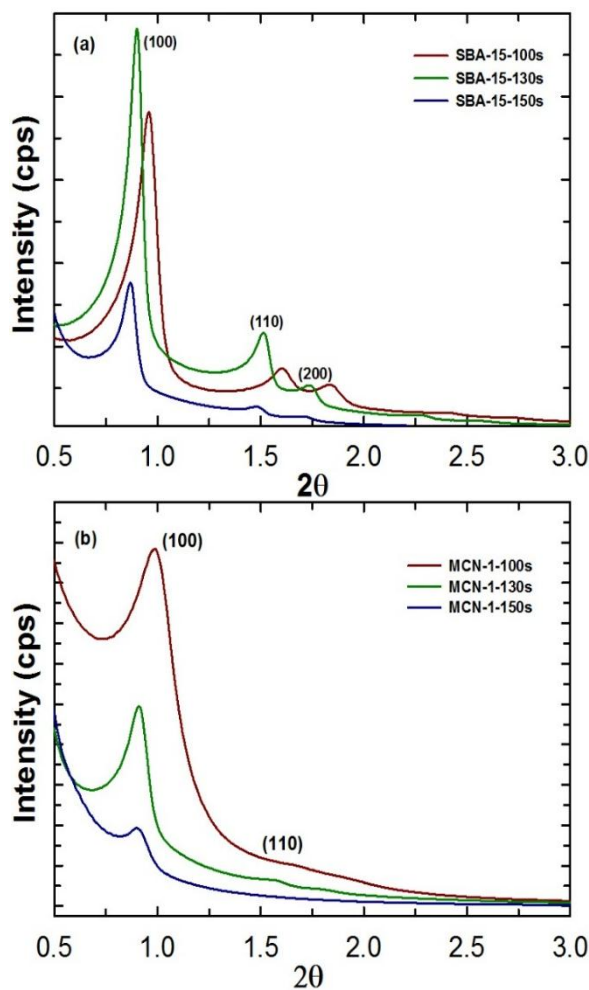


**Fig. 1:** Low angle powder X-ray diffraction patterns of (a) SBA-15-Ts silica templates and (b) MCN-1-Ts samples.

The increase of the unit cell constant of the samples with increasing synthesis temperature can be explained as follows: when the synthesis temperature is increased, dehydration of polyethylene oxide units surrounded by hydration spheres takes place. This would increase the length of the hydrophobic tail of the surfactant by coupling with the already existing hydrophobic polypropylene oxide moieties of the surfactant which is mainly responsible for creating the large mesoporosity in the samples. Moreover, it is known that the nonionic surfactant P123 is stable up to 130 °C and starts to decompose into smaller fragments at temperature higher than 130 °C. These small polymeric fragments also contribute to the enlargement of pores and the unit cell constant as they act as swelling agents and expand the micelles.

**Figure 1b** shows the low angle powder XRD plots for MCN-1-Ts samples which also exhibit a sharp peak and two low angle peaks. These peaks can be indexed to the (100), (110) and (200) reflections

which are associated with the hexagonally ordered mesostructures with a space group of  $p6mm$ . The presence of multiple peaks at lower angles clearly confirms the successful replication of the structure of SBA-15 silica template into MCNs. Interestingly, the peaks are shifted towards lower angle as the synthesis temperature or pore size of the SBA-15-Ts is increased. As observed in case of silica template material, the peak shift is more pronounced in MCN-1-150s as compared to the other two samples. Further, the intensity of the higher order peaks for MCN-1-150s is much lower as compared to that for MCN-1-100s and MCN-1-130s which indicates a slight structural disorder in the sample. For MCN-1-150s, the lower structural order may be attributed to the incomplete filling of the large mesopores of the SBA-15-150s with the carbon and nitrogen sources. Fig. 1S shows the high angle XRD patterns for MCN-1-Ts samples. These samples exhibit a broad peak at 2 theta values close to  $24.8^\circ$ , confirming the turbostratic ordering of carbon and nitrogen atoms in the graphene layer [11].

**Table 1.** Textural parameters and CO<sub>2</sub> adsorption capacities of SBA-15-Ts and MCN-1-Ts samples.

Sample	$a_0$ (nm)	$d$ (nm)	S.A (m <sup>2</sup> / g)	PD <sup>a</sup> (nm)	PV (cm <sup>3</sup> / g)	<sup>b</sup> CO <sub>2</sub> adso rbed (mm ol/g)
SBA-15-100s	10.63	9.25	710	8.4	1.11	12.4
SBA-15-130s	11.32	9.85	506	11.25	1.24	10.1
SBA-15-150s	11.74	10.21	388	11.29	1.19	8.4
MCN-1-100s	10.38	9.03	621	3.76	0.67	12.9
MCN-1-130s	11.16	9.71	678	4.99	0.87	16.5
MCN-1-150s	11.32	9.85	518	5.94	0.76	12.3
Activated carbon	-	-	747	5.3	0.41	3.7
MWCN-T	-	-	250	3.2	0.31	5.6

<sup>a</sup>Pore diameter calculated from the adsorption branch. <sup>b</sup>Adsorption measured at 0 °C and 30 bar using dry CO<sub>2</sub> gas.

**Figure 2a** shows the N<sub>2</sub> adsorption isotherms of the silica template SBA-15-Ts whereas the corresponding textural parameters are given in Table 1 and Table 1S. All the template materials show Type IV adsorption isotherm with a sharp capillary condensation step and a H1 hysteresis loop, which is typical of mesoporous materials with well-ordered large and cylindrical type pores. As the synthesis temperature is increased, the capillary condensation step is shifted from lower relative pressure to higher relative pressure, revealing the huge expansion of the pore size. The pore diameter of the samples increases from 8.4 to 11.29 nm upon increasing the synthesis temperature from 100 to 150 °C. On the other hand, the specific surface area of the materials decreases with increasing the synthesis temperature. The pore volumes of the samples are in the range of (1.11 to 1.29 cm<sup>3</sup>/g) which is quite similar to that of the samples prepared under dynamic conditions [12] (Table 1). Among the materials studied, SBA-15-130s exhibits the highest pore volume which might

be attributed to the excellent structural order and the large pore diameter.

The N<sub>2</sub> adsorption-desorption isotherms of MCN-1-Ts samples are shown in **Figure 2b**. It is clear from the isotherms of MCN-1-Ts samples that these materials also exhibit type IV isotherm with a capillary condensation step at the higher relative pressure, which indicates the presence of mesopores in the sample and further reinforces our claims about the successful replication of the structure of the templates to MCN-1-Ts. It can be seen from Table 1 that the pore diameter of the samples increases in the following order: MCN-1-100s > MCN-1-130s > MCN-1-150s (SI Fig. 2S). The utilization of the template with the large pore diameter offers the material with a large pore diameter. The specific surface area and the pore volume of the MCN-1-130s are much higher than those of other samples studied in this work, which may be attributed to the excellent structural order and better textural parameters of the SBA-15-130s template.

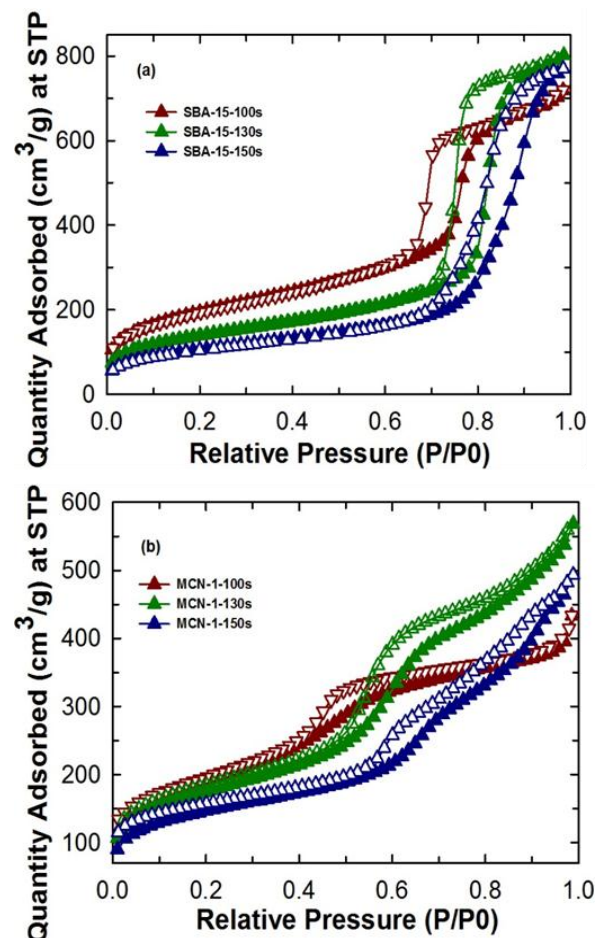


**Fig. 2:** Nitrogen adsorption isotherms for (a) SBA-15-Ts, and (b) MCN-1-Ts samples.

One of the highlights of this work is that the morphology of the materials can be easily controlled by varying the synthesis temperature and the stirring conditions. The morphology and the mesostructure of the MCN-1-Ts samples were studied by using HRSEM and HRTEM measurements. **Figure 3 (a-e)** show the SEM images for MCN-1-Ts samples prepared using the template synthesized at different temperatures. These images clearly demonstrate the presence of uniform rectangular morphology with small particle sizes for the MCN-1-Ts. These morphologies are similar to those of the parent silica template prepared by the static condition but much more uniform as compared to those of SBA-15

prepared under dynamic condition [12]. From the shape and size of the particles of all the samples prepared, it is quite clear that the morphology of the templates is replicated into the MCN-1-Ts samples and static condition is playing a crucial role in controlling the particle morphology including the size and shape. It should be noted that MCN-1-100s consists of uniform but bent rod shaped morphology which are cross-linked and thinner (Figure 3a, 3b) as compared to MCN-1-130 (Figure 3c, 3d) and MCN-1-150s (Figure 3e, 3f). On the other hand, MCN-1-130s exhibits uniform rod shaped particles with almost equal dimensions and are highly dispersed. Among the three samples, MCN-1-130s stands out in terms of uniformity of particle morphology. Interestingly, the size of the particles increases with increasing the synthesis temperature of the templates. This could be due to the fact that the higher temperature always reduces the surface curvature of the micelles and further enhances the interaction between the micelles and the silica species due to the quick condensation, which significantly increases the particle size. **Figure 4 (a-e)** show the HR-TEM images of MCN-1-100s, MCN-1-130s and MCN-1-150s samples. From the TEM images, it is clear that all the MCN-1-Ts samples exhibit well-ordered mesopores with a rectangular rod shaped morphology which is consistent with the data obtained from the HRSEM. It should be noted however that MCN-1-150s exhibits ordered mesopores but at a lower level compared to the samples MCN-1-100s and MCN-1-130s (**Figure 4c-4d**), which is again supported by the data obtained from XRD and nitrogen isotherm.

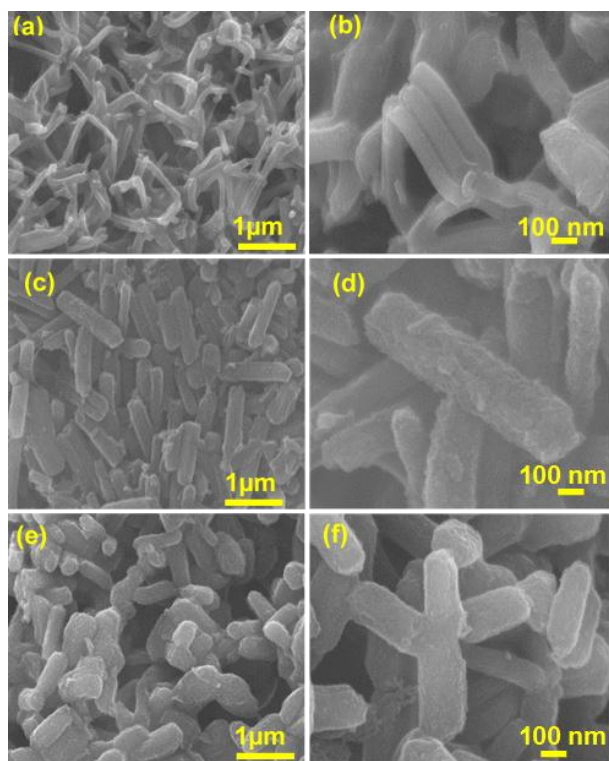


**Fig 3:** HRSEM images of (a,b) MCN-1-100s, (c,d) MCN-1-130s, and (e,f) MCN-1-150s.

The nature and co-ordination of C and N atoms in the MCN-1-Ts samples were characterized by using XPS and FT-IR spectroscopic techniques (Supporting Information). The XPS survey spectra of the MCN-1-Ts samples reveal that the samples are composed of C and N with a very small quantity of oxygen (**SI Fig. 3Sa**). The presence of small quantity of oxygen could be attributed to the ethanol wash or adsorption of moisture or CO<sub>2</sub> by the samples. No shift in the binding energy values of C and N was observed for the MCN-1-Ts samples

with different particle size and diameters. The surface atomic composition for all the three samples is shown in **Table 2**. The absence of the Si in the XPS survey spectra confirms that the template was completely removed during the HF treatment. The chemistry of C and N in MCN-1-Ts samples was further investigated using high resolution core level C1s and N1s scans and the data are shown in (**SI Fig. 3Sb and 3Sc** respectively). The C1s spectrum was deconvoluted into four peaks with B.Es as 289.1, 287.6, 285.3 and 284.5 eV. The low energy peak at 284.5 eV is assigned to pure graphitic sites in amorphous CN matrix whereas the peak at 287.6 is assigned to sp<sup>3</sup> hybridized carbon atom, which may come from the ethanol that was used for the washing of MCN. On the other hand, the peak at 285.3 is attributed to sp<sup>2</sup> carbon atoms bonded to N atom inside the aromatic structure while the peak at 289.1 is assigned to sp<sup>2</sup> hybridized carbon in the aromatic ring attached to NH<sub>2</sub> groups [11-12,27].

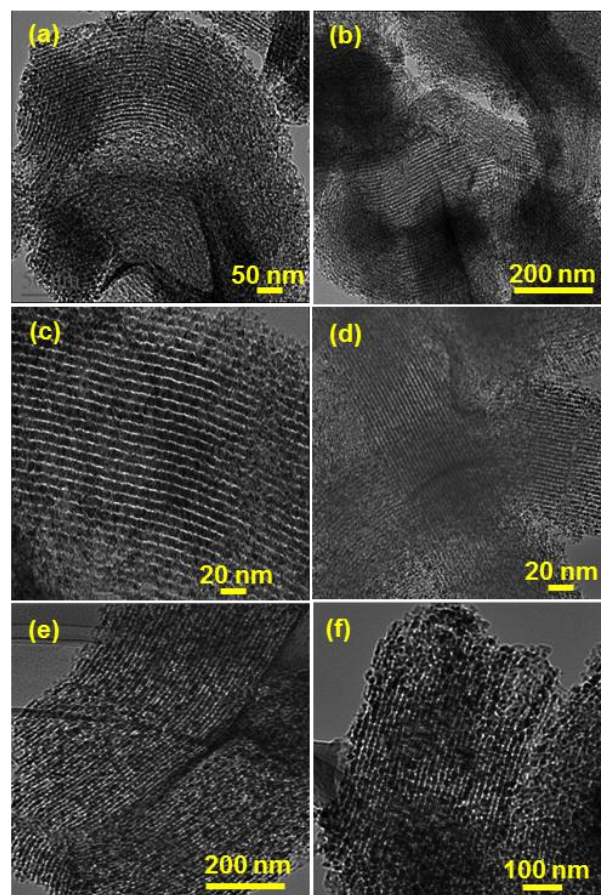


**Fig 4:** HRTEM images of (a,b) MCN-1-100s, (c,d) MCN-1-130s, and (e,f) MCN-1-150s.

**Table 2.** Atomic composition of MCN-1-Ts samples obtained from XPS measurement.

Sample	C (%)	N (%)	O (%)
MCN-1-100s	80.33	17.06	2.62
MCN-1-130s	77.4	18.88	3.73
MCN-1-150s	78.95	17.11	3.73

The N1s high resolution scan after deconvolution shows three well resolved peaks with B.Es as 398.2, 400.6 and 401.8 eV. The peak at the highest binding energy (401.8) is associated with terminal amino functions (C-H-N) whereas the peak at 398.2 eV is ascribed to nitrogen sp<sup>2</sup> bonded to carbon. The peak at 400.6 eV could be

attributed to N atoms trigonally bonded to all  $sp^2$  carbons, or to two  $sp^2$  carbon atoms and one  $sp^3$  carbon atom in an amorphous C-N network [11-13,27]. However, interestingly, the amount of nitrogen content in the sample MCN-1-130s is much higher than that of the other samples, which reveals that the structural order and fine morphology helps to avoid the thermal decomposition of N species from the CN framework in the wall structure of MCN-1-130s (Table 2). These results also reveal that MCN-1-130s has more number of free  $NH_2$  groups that are required for enhanced adsorption of  $CO_2$  molecules as compared to that of MCN-1-100s and MCN-1-150s. The nature of the functional group on the surface of MCN-1-Ts samples was also analyzed using FT-IR spectroscopy (SI Fig. 4S). The FT-IR scans of all the three samples show peaks that are consistent with the previous reported results of MCN-1 samples prepared using the SBA-15 templates [11-12].

### 3.1 $CO_2$ adsorption

The  $CO_2$  adsorption capacity of the pore tuned and morphology controlled MCN-1-Ts samples was evaluated at high pressures up to 30 bar and different analysis temperatures of 0, 10 and 25 °C. The choice of MCN as an adsorbent for  $CO_2$  was motivated by a number of reasons.  $CO_2$  being a Lewis acid is highly likely to interact with any Lewis base in an acid base neutralization reaction. The successful incorporation of highly basic nitrogen atoms in the mesostructures of MCN-1-Ts make it an ideal candidate for capture of an acidic molecule like  $CO_2$  through physisorption and chemisorption. Physisorption of  $CO_2$  takes place on the surface sites and mesoporous channels whereas the chemisorption is favored by the nitrogen or  $NH_2$  functionalities on the surface of the CN walls. Pore tuning, together with morphology control and better textural parameters also affect the  $CO_2$  adsorption capacity besides the number of  $NH_2$  groups on the surface. The nitrogen containing groups such as  $NH_2$  that are present on the surface of the MCN also act as Lewis basic sites thereby enable easy neutralization reaction with acidic  $CO_2$ .

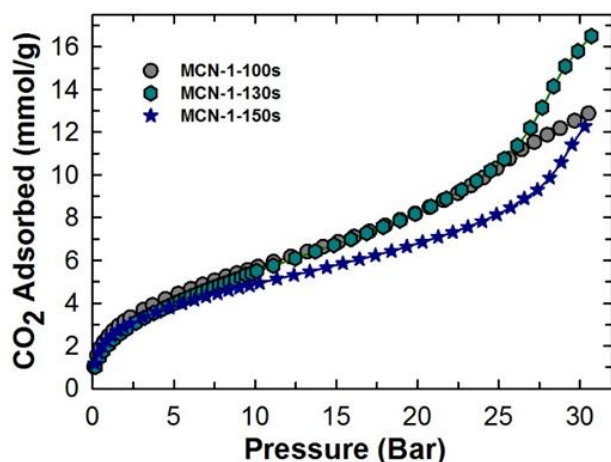


**Fig 5:**  $CO_2$  adsorption isotherms of MCN-1-Ts samples measured at 0 °C and pressure up to 30 bar.

**Figure 5** shows the  $CO_2$  adsorption isotherms of the MCN-1-Ts samples measured at 0 °C at different pressures. It can be seen from the **Figure 5** that MCN-1-130s registered the maximum  $CO_2$  adsorption of 16.5 mmol/g whereas MCN-1-100s and MCN-1-150s samples showed the  $CO_2$  adsorption capacities of 12.9 and 12.3 mmol/g, respectively under identical conditions. The higher adsorption capacity of MCN-1-130s could be attributed to the better structural and morphological order, higher surface area and pore volume and nitrogen contents as compared to those of MCN-1-150s and MCN-1-100s. For the purpose of comparison, we recorded the  $CO_2$  adsorption isotherms of commercially available activated carbon,

multi-walled carbon nanotubes (MWCNT), and large pore mesoporous silica SBA-15, MCN-1-130d (prepared under dynamic conditions) and mesoporous carbon nitride with 3D structure (MCN-7-130) at 0 °C and 30 bar (**Figure 6**) [13]. The  $CO_2$  adsorption was found to be in the following order: MCN-1-130s (16.5 mmol/g) > MCN-1-130d (14.6 mmol/g) > MCN-7-130 (13.5 mmol/g) > SBA-15-130s (10.1 mmol/g) > MWCNT (5.6 mmol/g) > AC (3.7 mmol/g). It is interesting to note that even though MCN-7-130[13] has 3D structure and much better textural parameters than the MCN-1-130s, the latter showed much better adsorption capacity. This could be attributed to the uniform and rectangular shaped morphology of the MCN-1-130s, revealing the role of morphology of the adsorbent on the adsorption capacity. **Table 3** shows the  $CO_2$  adsorption capacities of other reported materials such as polyethyleneimine (PEI) functionalized mesoporous capsules, PEI functionalized mesoporous silica KIT-6, zeolite like metal organic framework and MCN-7 measured under identical conditions [10,13,28-29]. Based on the values indicated in **Table 3**, it is evident that MCN-1-130s sample has superior  $CO_2$  adsorption capacity under identical temperature and pressure conditions. It is clear from all these results that overall  $CO_2$  adsorption capacity of a material is dictated not just by structure or structural parameters or functional moieties alone but the morphology also plays a key role in determining the adsorption capacity of the adsorbents. In order to understand the role of temperature on the adsorption of  $CO_2$  over MCN-1-Ts materials, the adsorption experiments were conducted at different temperatures.

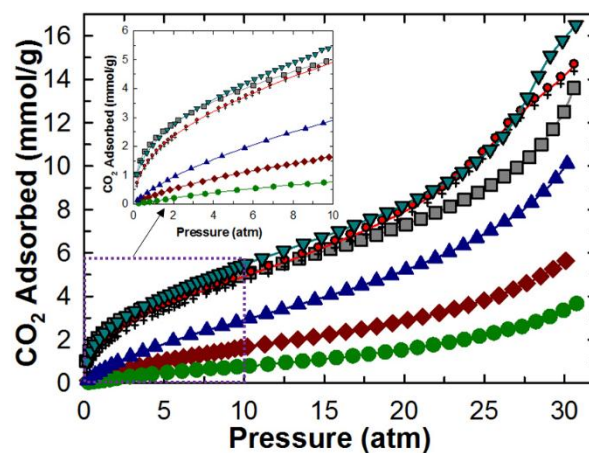


**Fig 6:** Comparison of  $CO_2$  adsorption capacities of different materials with MCN-1-130s sample measured at 0 °C and pressure up to 30 bar: (●) activated carbon, (◆) MWCNT, (▲) SBA-15-130s, (■) MCN-7-130, (▼) MCN-1-130D, and (▼) MCN-1-130s.

**Figure 7 (a-c)** show the adsorption isotherms of MCN-1-100s, MCN-1-130s and MCN-1-150s respectively at 0, 10 and 25 °C. We found that as the adsorption temperature was increased from 0 to 25 °C, the  $CO_2$  adsorption capacity of the materials decreased drastically. This clearly suggests that  $CO_2$  adsorption process is exothermic in nature. Further the strength of the interaction between the adsorbate and adsorbent was studied by calculating the heat of adsorption. As MCN-1-130s shows the highest adsorption capacity among the three samples, adsorption isotherms of MCN-1-130s samples were recorded at 0, 10 and 25 °C and 30 bar (**Figure 7b**). The isosteric heat of adsorption (**Figure 8**) of MCN-1-Ts sample was calculated from the Clausius-Clayperon equation using the three isotherms recorded at different temperatures and shown in **Table 3**. The samples register higher isosteric heat of adsorption at lower loading but decreases as the loading is increased. This observation can be explained based on the fact that at lower  $CO_2$  loadings, active nitrogen sites are mainly responsible for adsorption whereas other active sites including carbon sites and well-ordered structure facilitate higher adsorption at a higher

pressure. Similar trend in variation of isosteric heat with CO<sub>2</sub> loading was observed with MCN-7 with 3D structure [13].

Interestingly, MCN-1-150s shows the highest heat of adsorption followed by MCN-1-130s and MCN-1-100s which indicates that the adsorbate-adsorbent interaction is the strongest for MCN-1-150s sample, followed by MCN-1-130s and MCN-1-100s. This trend could be explained on the basis of easy accessibility of CO<sub>2</sub> molecules to the large pores of MCN-1-150s and high N% per unit surface area which favor the multilayer adsorption and strong adsorbent-adsorbate interaction respectively. In addition, the large micropore volume of the sample also support the strong interaction between the CO<sub>2</sub> molecules. However, the pore volume and the specific surface area of the MCN-1-150s, which are the key parameters to enhance the CO<sub>2</sub> adsorption capacity, are lower than those of MCN-1-130s (Table 1 and 1S). Therefore, highest CO<sub>2</sub> adsorption capacity was achieved for MCN-1-130s. It is interesting to note that the heat of adsorption of MCN-1-Ts samples is higher than that of MCN-7-130 although the later has a 3D cage type large pores which is expected to show a strong interaction with the CO<sub>2</sub> molecules. The higher heat of adsorption of MCN-1-Ts could be attributed to the uniform particle size and shape together with the large mesopores volume, which would allow the CO<sub>2</sub> molecules adsorb strongly with the surface and even the active sites at the deep internal part of the pores.

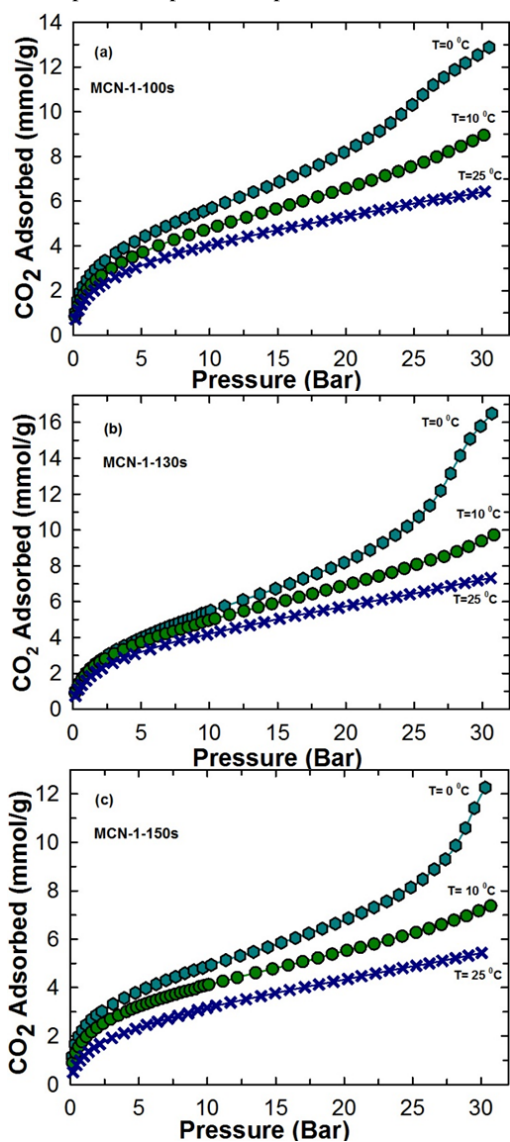


**Fig 7:** CO<sub>2</sub> adsorption isotherms at 0, 10 and 25 °C and pressure up to 30 bar for (a) MCN-1-100s, (b) MCN-1-130s, and (c) MCN-1-150s.

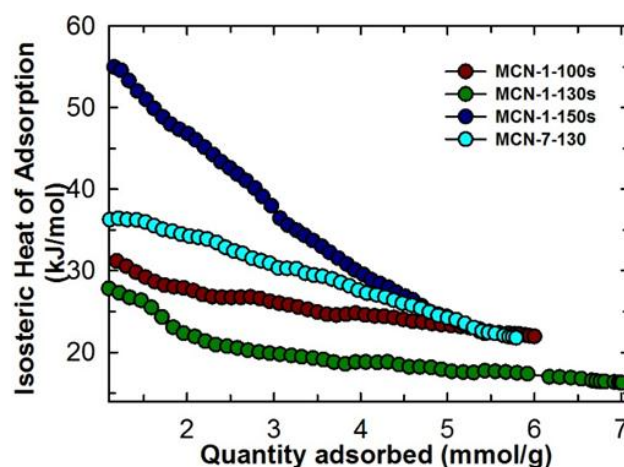


**Fig 8:** Variation of isosteric heat of adsorption with CO<sub>2</sub> loading for MCN-1-Ts samples and their comparison with MCN-7-130 sample [13].

Noteworthy, CO<sub>2</sub> adsorption capacity of MCN-1-Ts samples depends strongly on the surface area and pore volume of the samples when other factors are kept the same. Sample with higher BET surface area and pore volume gives the highest adsorption keeping the adsorption temperature and pressure same (**Figure 9**). This result is expected as higher surface would mean larger number of basic sites with free NH<sub>2</sub> groups resulting in greater adsorption. In order to check the recyclability, the samples were regenerated by heating under vacuum between 200–250 °C for 6–8 h. To our surprise, the regenerated samples did not show any structural collapse or loss of adsorption capacity. These results prove that the prepared MCN samples are promising adsorbents for CO<sub>2</sub> capture.

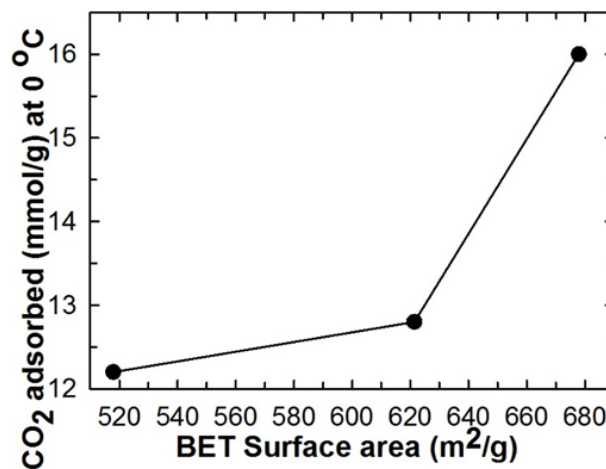


**Fig 9:** Effect of BET specific surface area on the quantity of CO<sub>2</sub> adsorption over MCN-1-Ts samples.

**Table 3.** Comparison of the CO<sub>2</sub> adsorption capacities of MCN-1-Ts samples with other reported materials.

Sample	T (°C)	Pressure (bar)	<sup>d</sup> CO <sub>2</sub>	Ref
--------	--------	----------------	------------------------------	-----

			(mmol/ g)	
<sup>a</sup> PEI-KIT-6	75	1.0	3.07	10
MC400/10PEI%83 <sup>b</sup>	75	0.101	4.91	29
Sod-ZMOF <sup>c</sup>	25	1.0	1.15	28
MCN-7-130	0	30.0	13.5	13
MCN-7-130	25	30.0	5.9	13
MCN-7-130	25	1.0	1.4	13
MCN-1-100s	0	30.0	12.9	PW
MCN-1-130s	0	30.0	16.5	PW
MCN-1-130s	25	30.0	7.31	PW
MCN-1-130s	25	1.0	1.61	PW
MCN-1-150s	0	30.0	12.3	PW
MWCNT <sup>e</sup>	0	30.0	5.63	PW
Activated Carbon	0	30.0	3.66	PW

<sup>a</sup>PEI: Polyethyleneamine ; <sup>b</sup>MC: mesoporous silica capsules; <sup>c</sup>ZMOF: zeolite like metal organic framework; <sup>d</sup>dry CO<sub>2</sub> gas ; <sup>e</sup>MWCNT : Multi-walled carbon nanotubes; PW : present work

#### 4. Conclusions

In this paper, we have reported the synthesis and CO<sub>2</sub> adsorption performance of highly ordered mesoporous carbon nitride with uniform particle morphology and tunable pore diameters from the SBA-15 template prepared by static method. The prepared materials exhibited high specific surface area, large pore volume and well-ordered porous structure with highly uniform particle morphology. The pore size of the samples can be tuned from 3.76 to 5.94 with the simple adjustment of the pore diameter of the template. With this strategy, a variety of mesoporous carbon nitride with different structure and pore diameters can be easily fabricated. These materials were employed as adsorbents for CO<sub>2</sub> molecules and the results were compared with other mesoporous materials including 3D mesoporous carbon nitride. In comparison to the 3D cage type MCN-7-130 (13.5 mmol/g at 0 °C and 30 bar), MCN-1-130s sample showed much higher CO<sub>2</sub> adsorption capacity (16.5 mmol at 0 °C and 30 bar, which is higher than other mesoporous and porous samples. The higher adsorption capacity was related with the well-ordered structure with uniform particle morphology, and higher specific surface area and large pore volume. We also demonstrated that a combination of low CO<sub>2</sub> adsorption temperature and high adsorption pressure is a favorable condition for higher CO<sub>2</sub> adsorption. At higher temperature, CO<sub>2</sub> adsorption capacity reduced significantly possibly due to the physically adsorbed CO<sub>2</sub> molecules. It has also been found that these materials possess excellent recyclability and could be re-generated by heating under vacuum between 200-250 °C for 6-8h without suffering any structural collapse or loss of adsorption capacity and thus promising to be an excellent adsorbent for large scale industrial application involving capture and conversion of CO<sub>2</sub> molecules.

**Table 4.** Isothermic heat of adsorption of MCN-1-Ts samples.

Sample	Isothermic heat of adsorption range <sup>a</sup> (kJ/mol)
MCN-1-100s	31.1 – 22.0
MCN-1-130s	27.9 – 16.3
MCN-1-150s	54.9 – 22.3
MCN-7-130	34.9 – 24.0 <sup>[13]</sup>

<sup>a</sup>Isothermic heat of adsorption calculated from Clausius-Clapeyron equation using the isotherms recorded at 0, 10, and 25 °C.

#### Acknowledgements

One of the authors A. Vinu is grateful to ARC for the award of future fellowship and the University of Queensland for the start-up grants. The authors also acknowledge the facilities, and the scientific and technical assistance, of the Australian Microscopy

and Microanalysis Research facility at the centre for microscopy and microanalysis (CMM), the University of Queensland. The project was also financially supported by King Saud University, Vice Deanship of Scientific Research Chairs.

#### Notes and references

<sup>a</sup>Australian Institute for Bioengineering and Nanotechnology (AIBN), The University of Queensland, Brisbane, QLD, Australia.

<sup>b</sup>Petrochemical Research Chair, Department of Chemistry, College of Science, King Saud University, Riyadh 11451, Saudi Arabia.

<sup>c</sup>Department of Chemistry and Nanoscience, Ewha Womans University, Seoul, South Korea

1. C.-H. Y. C. -H. Huang, C.-S. Tan, *Aerosol and Air Quality Research*, 2012, **12**, 745.
2. D. Qian, C. Lei, E. -M. Wang, W.-C. Li, A.-H. .Lu, *ChemSusChem*, 2014, **7**, 291.
3. K. Ahmad, O. Mowla, E. M. Kennedy, B. Z. Dlugogorski, J. C. Mackie, M. Stockenhuber, *Energy Technol.*, 2013, **1**, 345.
4. Y. Zhao, K. X. Yao, B. Teng, T. Zhang, Y. Han, *Energy Environ. Sci.*, 2013, **6**, 3684.
5. Y. Jing, L. Wei, Y. Wang, Y. Yu, *Microporous and Mesoporous Materials*, 2014, **183**, 124.
6. R. Sanz, G. Celleja, A. Arencibia, E. S. Sanz-Perez, *Applied Surface Science*, 2010, **256**, 5323.
7. R. Sanz, G. Calleja, A. Arencibia, E. S. Sanz-Perez, *Microporous and Mesoporous Materials*, 2012, **158**, 309.
8. Z. Wu, P.A. Webley, D. Zhao, *Journal of Materials Chemistry*, 2012, **22**, 11379.
9. X. Zhu, P. C. Hillesheim, S. M. Mahurin, C. Wang, C. Tian, S. Brown, H. Luo, G. M. Veith, K. S. Han, E. W. Hagaman, H. Liu, S. Dai, *ChemSusChem*, 2012, **5**, 1912.
10. W.-J. Son, J.-S. Choi, W.-S. Ahn, *Microporous and Mesoporous Materials*, 2008, **113**, 31.
11. A. Vinu, K. Ariga, T. Mori, T. Nakanishi, S. Hishita, D. Golberg, Y. Bando, *Adv. Mater.*, 2005, **17**, 1648.
12. A. Vinu, *Adv. Funct. Mater.*, 2008, **18**, 816.
13. K. S. Lakhi, W. S. Cha, S. Joseph, B. J. Wood, S.S. Aldeyab, G. Lawrence, J.-H. Choy, A. Vinu, *Catalysis Today*, 2015, **243**, 209.
14. Y. Wang, F. Zhang, Y. Wang, J. Ren, C. Li, X. Liu, Y. Guo, Y. Guo, G. Lu, *Materials Chemistry and Physics*, 2009, **115**, 649.
15. C. Yu, J. Fan, B. Tian, D. Zhao, G.D. Stucky, *Adv. Mater.*, 2002, **14**, 1742.
16. P. S.-Winkel, P. Yang, D. I. Margolese, B.F. Chmelka, G.D. Stucky, *Adv. Mater.*, 1999, **11**, 303.
17. K. Kosuge, T. Sato, N. Kikukawa, M. Takemori, *Chem. Mater.*, 2004, **16**, 899.
18. A. Sayari, B.-H. Han, Y. Yang, *J. Am. Chem. Soc.* 2004, **126**, 14348.
19. L.-C. Sang, A. Vinu, M.-O. Coppens, *Journal of Materials Chemistry*, 2011, **21**, 7410.
20. A. Vinu, C. Sterb, V. Murugesan, M. Hartmann, *J. Phys. Chem. B*, 2003, **107**, 8297.
21. A. Vinu, M. Miyahara, K. Ariga, *J. Phys. Chem. B*, 2005, **109**, 6436.
22. M. Hartmann, A. Vinu, G. Chandrasekar, *Chem. Mater.*, 2005, **17**, 829.
23. A. Vinu, M. Miyahara, V. Sivamurugan, T. Mori, K. Ariga, *Journal of Materials Chemistry*, 2005, **15**, 5122.
24. A. Vinu, K.Z. Hossian, G.S. Kumar, K. Ariga, *Carbon*, 2006, **44**, 530.

25. L.-C. Lang, A. Vinu, M.-O. Coppens, *Langmuir*, 2011, **27**, 13828.
26. A. Vinu, M. Miyahara, K. Ariga, *Journal of Nanoscience and Nanotechnology*, 2006, **6**, 1510
27. Q.-F. Deng, L. Liu, X.-Z. Lin, G. Du, Y. Liu, Z.-Y. Yuan, *Chemical Engineering Journal*, 2012, **203**, 63.
28. C. Chen, J. Kim, D.-A. Yang, W.-S. Ahn, *Chemical Engineering Journal*, 2011, **168**, 1134.
29. G. Qi, Y. Wang, L. Estevez, X. Duan, N. Anako, A.-H.A. Park, W. Li, C.W. Jones, E.P. Giannelis, *Energy & Environmental Science*, 2011, **4**, 444.